Target Alignment in Astra-Gemini

Contact *nicola.booth@stfc.ac.uk*

Nicola Booth, Oliver Ettlinger, David Neely, Rajeev Pattathil, Andrew Sellers, Dan Symes

Central Laser Facility,
STFC Rutherford Appleton Laboratory, Harwell Oxford, Didcot

Introduction

The challenge of positioning targets at the focus of a laser with an accuracy of less than a micron is a significant one. The positioning of targets is performed in many different ways[1] and typically involves long working distance microscopes, retro-reflection or absolute positioning. Experimental data relies upon accurate knowledge of the on target intensity in order to properly analyse and simulate the data obtained during an experiment[2]. This is a particular problem in Astra-Gemini, as utilising short focal length parabolas (typically f/2 focussing) means that, in order to reproducibly access the highest intensities available, targets must be positioned with < 8 micron accuracy. If we are to move to higher intensities through even shorter focal length optics, the issue of accurate alignment of a target must be addressed.

Rear surface imaging

In Astra-Gemini we are designing two complimentary systems to enable accurate target alignment. The first of these is an upgraded camera system (the current design is discussed in ref 3), the design is shown in figure 1. This will allow us to ensure that the rear surface of the target is positioned to < few microns accuracy and will also be used to image the focal spot of the Astra-Gemini laser. It consists of a 1" achromat lens, which is relatively cheap and easily replaceable if it is destroyed by debris or accidentally hit by the laser. There are three non-polarising beam splitter cubes (NPBS) attached using c-tube. NPBS 1 has a collimated 800nm fibre laser input, which is the same wavelength as the Astra-Gemini laser, to ensure that no chromatic offsets are required, and a CCD camera to observe the near field of the reflected beam. NPBS 2 is attached to a far field camera, to look at the focal spot from Gemini, and the focus of the 800 nm fibre beam on the rear surface of the target. The final NPBS 3 has an LED input also at 800 nm, to allow imaging of any features on the rear surface of the target, and to see the outline of any target mounts, to enable us to position the centre of the target correctly. Figure 2a shows an image obtained of the rear surface of a gold target using this LED illumination. Small features such as dust and wrinkles on the surface of any target type can be easily imaged.

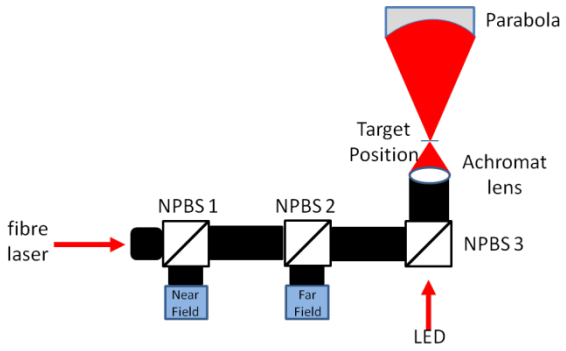

Figure 1. Design of the new rear surface imaging system to be implemented in Gemini.

By combining the near field and far field cameras into this system, it is possible to also use this as a diagnostic to position the angle of the target is correctly, as an angle on the target will produce a far-field pointing shift, which can then be corrected by adjusting the target. Figure 2b shows an example of the far-field focal spot that can be imaged using this system, with the achromat lens giving a spot of ~ 30 microns FWHM in this configuration.

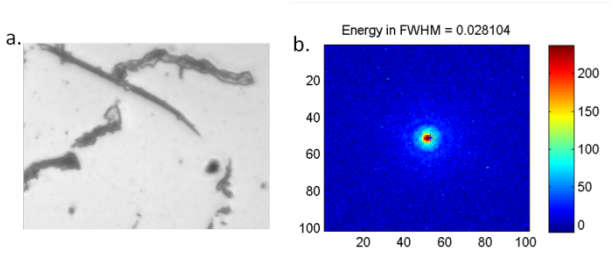

Figure 2. Features imaged on the rear surface of a gold target using the new design of camera system. Focal spot image of the 800 nm fibre laser focussed at the target position showing a 30 μm focal spot

Three colour interferometry

We are also planning to implement an interferometer based on a Mach-Zehnder[4] design to aid us in positioning targets to micron and potentially sub-micron precision. When using a coherent broadband light source, the Mach-Zehnder works by producing interference patterns when both of the arms of the interferometer are the same length. If there are differences in the path length, or if there is any tip or tilt on the mirrors of either arm then the interference pattern will alter in a manner dependant on the movement. The accuracy of this method can be extended as far as (λ/10). However, with conventional interferometry, with a single wavelength it impossible to distinguish one fringe from the next, vastly limiting its overall usability for the purposes of a distance measurement. The ideal situation would be to use broad bandwidth "white light" interferometry. However, with the variety of targets used in Gemini, that would require a very high brightness source.

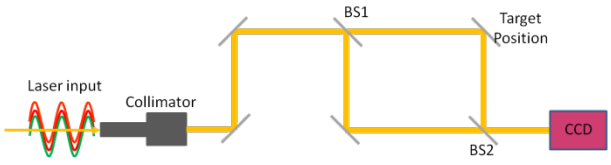

Figure 3. Layout of the Mach-Zehnder Interferometer to be implemented in Astra-Gemini.

The system that we are currently developing is a three colour interferometer, with equally powered lasers of 532 nm, 635 nm and 658 nm wavelength from different sources and are

combined using a wavelength division multiplexer[5]. The multi-wavelength output of this fibre is then collimated to 10mm and is input into the Mach-Zehnder interferometer (figure 3).

The three different colours produce a distinctive interference pattern, unlike that obtained with a single colour interferometer, which have purely light and dark fringes. Figure 4 shows the interference pattern obtained with a colour CCD camera when the interferometer is perfectly aligned and two images of interference patterns obtained with a vertical tilt or a horizontal twist imposed on the target position. With a vertical tilt imposed, the fringes start to turn in a clockwise or anti-clockwise fashion, depending on the direction of tilt. When a horizontal twist is imposed, this then changes the spacing of the fringes, either narrowing the fringes or increasing the spacing of them, again dependant on the direction of movement.

Figure 4. Interference patterns of the three colour interferometer; a. when the interferometer is perfectly aligned, b. with a vertical tilt on the target mirror showing a rotation of the fringes and c. with a horizontal twist on the target mirror, narrowing the spaces between the fringes.

As can be seen from the lineouts in figure 5, there is a distinct pattern to the fringes, which changes as the length of the target arm of the interferometer is changed. This is a different pattern than the regular intensity fringes that are usually seen with a single colour interferometer, and as such, make it easier to distinguish between the fringes when making a distance measurement. After a move of 1 micron, the fringe intensity has reduced, and the central fringes have stayed in place. It is possible to see the tracking of some of the features in the lineouts from the reference pattern to the pattern after a 1 micron movement, and it is these changes that will enable us to reposition the target at best focus.

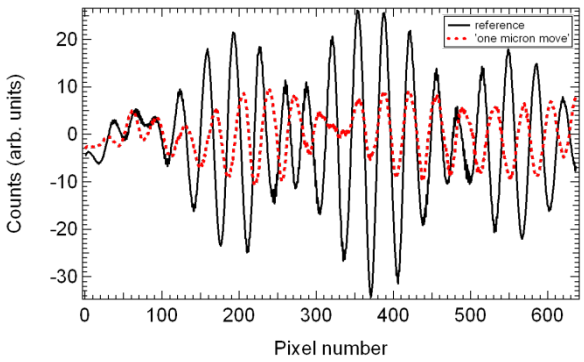

Figure 5. Lineouts of the interference images at the reference position (—), and after moving the target by 1 micron (-----).

These two complimentary techniques when used together will be a powerful method of ensuring that your target is not only positioned at the correct distance from your focussing optic, but also with no angle on the target. This is particularly important for any experimental measurements that are directional, such as proton acceleration[6] and harmonic generation[7].

Conclusions

It is hoped that, on commissioning into the target chamber, these two methods of target alignment will allow us a significant improvement in our ability to place targets accurately at the laser focus. It is also hoped that this will enable a significant reduction in the time taken to align a target to make better use of the Gemini repetition rate.

It is hoped that both these target alignment systems will be commissioned in Astra-Gemini in early 2014, ready for use on solid target campaigns shortly after, where the aim will be to shoot thin foils at the highest available intensities.

References

1. I. Spencer et al, Phys. Rev. E, **67**, 4, 046402, 2003
2. C. Brenner et al, Laser and Particle Beams, **29**, p345-351, 2011
3. D. Carroll et al, *An imaging system for accurate target positioning for fast focusing geometries*, CLF Annual Report, 2011-2012
4. Zehnder, Ludwig (1891). . *Zeitschrift für Instrumentenkunde* **11**: 275–285; Mach, Ludwig (1892). *Zeitschrift für Instrumentenkunde* **12**: 89–93
5. http://www.ozoptics.com/ALLNEW_PDF/DTS0089.pdf
6. M. H. Xu et al, Appl. Phys. Lett. 100, 8, 084101, 2012
7. B. Dromey et al, Phys. Rev. Lett, 102, 22, 225002, 2009

Measurement of the difference in the Gemini gate valve windows thickness by its effect on timing between the North and South beams

Contact *david.carroll@stfc.ac.uk*

D. C. Carroll

Central Laser Facility, STFC RAL, Oxfordshire, OX11 0QX, UK

C. D. Murphy

School of Physics and Astronomy, The University of Edinburgh, Edinburgh, EH9 3JZ, UK

Introduction

The Astra Gemini laser has two separate beams, referred to as North and South, which are delivered to the target area via two separate compressor chambers. When the target vacuum chamber is at air to keep the compressor chambers under vacuum gate valves are closed between the chambers. These gate valves have full aperture sapphire windows which enables full beam alignment in the target chamber.

For experiments which are using both beams the relative timing of the two beams is critical, especially if temporal overlap is required as both beams can be compressed down to pulse durations of 40 fs. A relatively easy technique of timing pulses that are tens of femtoseconds is to break down the air with one beam and image this break down with the second beam. Please note that both beams are focused and spatially overlapped for this, the imaging beam's diameter is artificially reduced so that the focal spot it produces can't break down the air and the power of the break down beam is reduced until it is only just able to cause the air to breakdown at focus. The relative timing is adjusted until the imaging beam is imaging the start of the plasma breakdown. The plasma from the breakdown is much longer lived than the duration of the laser pulse it is easy to tell if the imaging beam is late or early.

If this is done in the Gemini chamber at air and the experiment will be at vacuum then a correction will be needed to the timing to account for any difference in thickness of the two sapphire gate valve windows. In this article we present work where we implemented a variation of this timing technique to perform the timing under vacuum and which enabled the difference in relative thickness of the gate valve windows to be measured.

Setup

Both the North and South Gemini beams were focused by two F/2 off-axis parabolic mirrors onto the same spatial location defined by the tip of a wire and with the two beams orthogonal to each other. The South beam diameter was then reduced down to 3 mm to form a large approximately 100 µm focal spot that would probe the higher intensity North beam focal spot interaction.

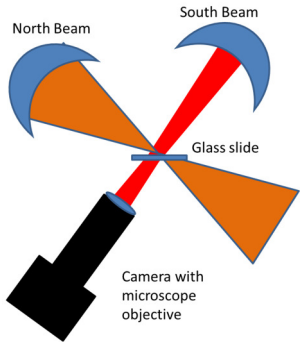

Fig 1: Schematic of the experimental setup

A glass microscope slide target was then placed with the front surface at the focus of the two Gemini beams. The imaging objective system looking at the South beam spot was corrected to account for the glass plate thickness. The laser energy was then adjusted until the North beam was only able to damage the glass plate at the tightest focus. Between shots the glass slide was moved vertically so that a fresh area of glass was interacted with each time.

Results

Initially the gate valves for the North and South beams were kept closed though the target chamber was at vacuum. The relative timing of the two beams is varied by moving a time slide on one of the beam lines. If damage or plasma is observed in the glass in the probe image of the South beam then the South beam is later than the North beam. If there is no damage or plasma observed in the probe image this means the South beam is arriving before the North beam. This is a similar technique to that used by M. Harmand *et al* who used to time an optical laser with a free electron laser [1]. By alternating on either side and reducing the changes in the relative timing the temporal overlap can be found. The measurements are then repeated but with the gate valves for the two beams open, results for both cases are shown in Fig 2. The difference in the time slide positions for the two set of measurements is proportional to the difference in thickness of the two time slides.

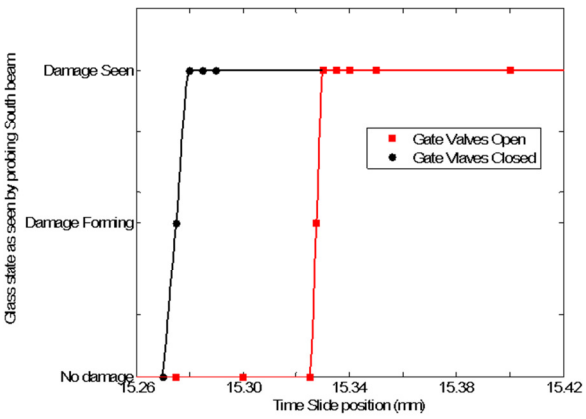

Fig 2: Presence of damage in glass as a function of time slide position. Black circles are for when the gate valves are closed and the red squares are for when the gate valves are open. Larger time slide values move the South beam later in time with respect to the North Beam.

It was found that with the gate valves closed the South beam had to be moved earlier in time with respect to the North beam (lower values on time slide) than when the gate valves are open. This implies that the South beam is being delayed more than the North beam and is therefore passing through more gate valve material which the light travels slower within. The difference in timeslide position is 52.5 ± 2.5 µm which is a total path

difference of 105 ± 5 µm which is equivalent to 350 ± 17 fs timing difference in air.

The gate valves are made of sapphire which has a refractive index of 1.75 for the extraordinary axis and 1.76 for the ordinary axis for 800 nm wavelength light. This means that a timing difference of 350 ± 17 fs is equivalent to 60 ± 3 µm of sapphire. The difference between the extraordinary and ordinary axes is within the error of the measurement.

Conclusion

The North and South beams of Astra-Gemini were overlapped temporally under vacuum. This was done for both with the gate valves open and with the gate valves closed. The difference in the relative timing of the two beams enabled the difference in the gate valve thickness to be calculated. It was found that the South beam gate valve is 60 ± 3 µm thicker than the North beam gate valve. The effect this has on timing is that the South beam is delayed by an additional 350 ± 17 fs when the gate valves are close.

Acknowledgements

We acknowledge the expert support provided by the staff at the Central Laser Facility of the Rutherford Appleton Laboratory.

Acknowledgements

[1] M Harmand *et al* 2012 *JINST* **7** P08007

Analysis of thermal lens in the Gemini amplifier under high repetition pump rate

Contact *Oleg.Chekhlov@stfc.ac.uk*

O.Chekhlov, C. Hooker, C. Hernandez-Gomez
Central Laser Facility, STFC Rutherford Appleton Laboratory
M.D. Fitton, A. Atherton
High Power Targets Group, Applied Science Division, STFC

Introduction

Astra Gemini is a chirped pulse amplification laser system [1] based on a large aperture Ti:Sapphire active element, and has been in been in operation for six years. However, recent developments towards a high repetition rate petawatt laser amplifier required a more detailed analysis of various operational parameters. In this paper we present the results of a computer analysis of thermal distribution within the crystal at room temperature, and discuss thermal lens compensation via the optical design of the Gemini amplifier.

Modelling of thermal loading in the Ti: Sapphire crystal

Recent progress in the development of kilowatt average power pump lasers brings into question the suitability of Gemini for high repetition rate pulse amplification. The current design allows amplification of stretched femtosecond pulses in the 50mm diameter beam at a low (1/20 sec) repetition rate of 60J pump pulses. For our development towards a 10 Hz repetition rate the existing Ti:Sapphire crystal from Gemini amplifier has been chosen for modelling. The crystal is shaped as a disc 90mm in diameter and 25mm in length. Optical pumping is arranged from both flat sides of the disc [2], with a 50mm diameter pumped area centered in the middle of the crystal. Pumping from two sides causes a slight dependence of power deposition in the crystal along its length. The thermal load on the crystal is governed by the quantum deficit between the pump wavelength (530nm) and the peak wavelength (790nm) of Ti:Sapphire fluorescence.

An analysis of the thermal distribution in the crystal at a steady state has been made by the High Power Targets Group using the ANSYS software tools. Crystal cooling was modelled by a flow of liquid at 15^0C, with heat transfer coefficient 5000 W/m*K at the round edge of the crystal.

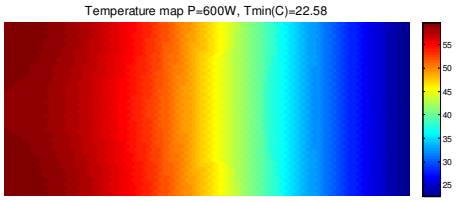

Figure 1. Temperature distribution map along 25mm (vertical) length and 45mm (horizontal) radius of the Ti:Sapphire crystal. The map corresponds to 600W of input pump power.

The main feature of the edge cooling – the radial distribution of temperature – can be seen in figure 1. The left-hand side of the map represents distribution at the center of the crystal, the right-hand side represents temperature at its edge. Power deposition at the center of the crystal together with edge cooling gives rise to the crystal temperature at the center. The optical path difference was calculated according to the temperature map to estimate the change in optical properties of the active element, while the change in optical path was calculated using the thermal change of both the crystal length andits refractive index.

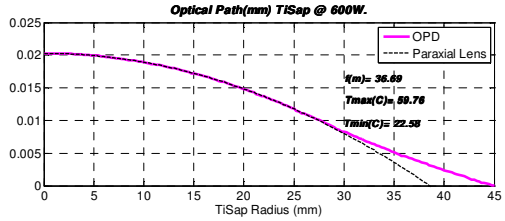

Figure 2. Variation of optical path difference (OPD) in dependence on crystal radius. The black line is the paraxial lens OPD dependence.

Figure 2 shows that the radial dependence of the optical path (the magenta line in the figure 2) can be approximated by the paraxial lens formula (the black line). The focal length of the thermal lens at 600W input pump power has been estimated as f~ 36.7 m for the temperature difference between the center and edge of the crystal ΔT~37.18^{0}C. The results in figures 1 and 2 correspond to the natural convection at the faces of the crystal at 20^0C and 20W/m^{2}K. More intensive cooling at the faces has also been modelled, but this only slightly altered the general radial temperature dependence due to actual size of the crystal and geometry of the pump region.

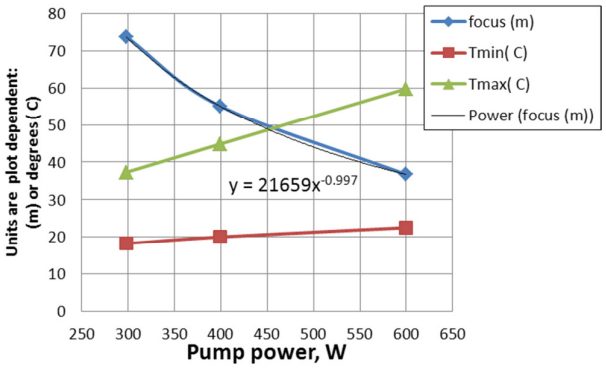

Figure 3. Variation of the thermal lens focal length (blue), minimum (red) and maximum (green) temperatures of the Ti:Sapphire crystal with increasing total input power.

The dependence between thermal focal length and pump power is presented in figure 3. This shows that the steady state temperature in the crystal increases with pump power. It is also noted that even at the heat transfer rate of 5000 W/m*K there is a noticeable increase in temperature between the center of the Ti:Sapphire crystal and its edge.

Optical modelling of the Gemini amplifier

The design of the Gemini amplifier is based on four-pass amplification through the crystal; three telescopes are used for image relay between each path [2]. The observed thermal lensing in the Ti:Sapphire at high repetition rate pumping needs to be compensated to keep the amplified beam size matched to the pumped area at each pass through the crystal. One method of compensating for this lensing effect is to use an adaptive optics (AO) deformable mirror. However, thermal lens

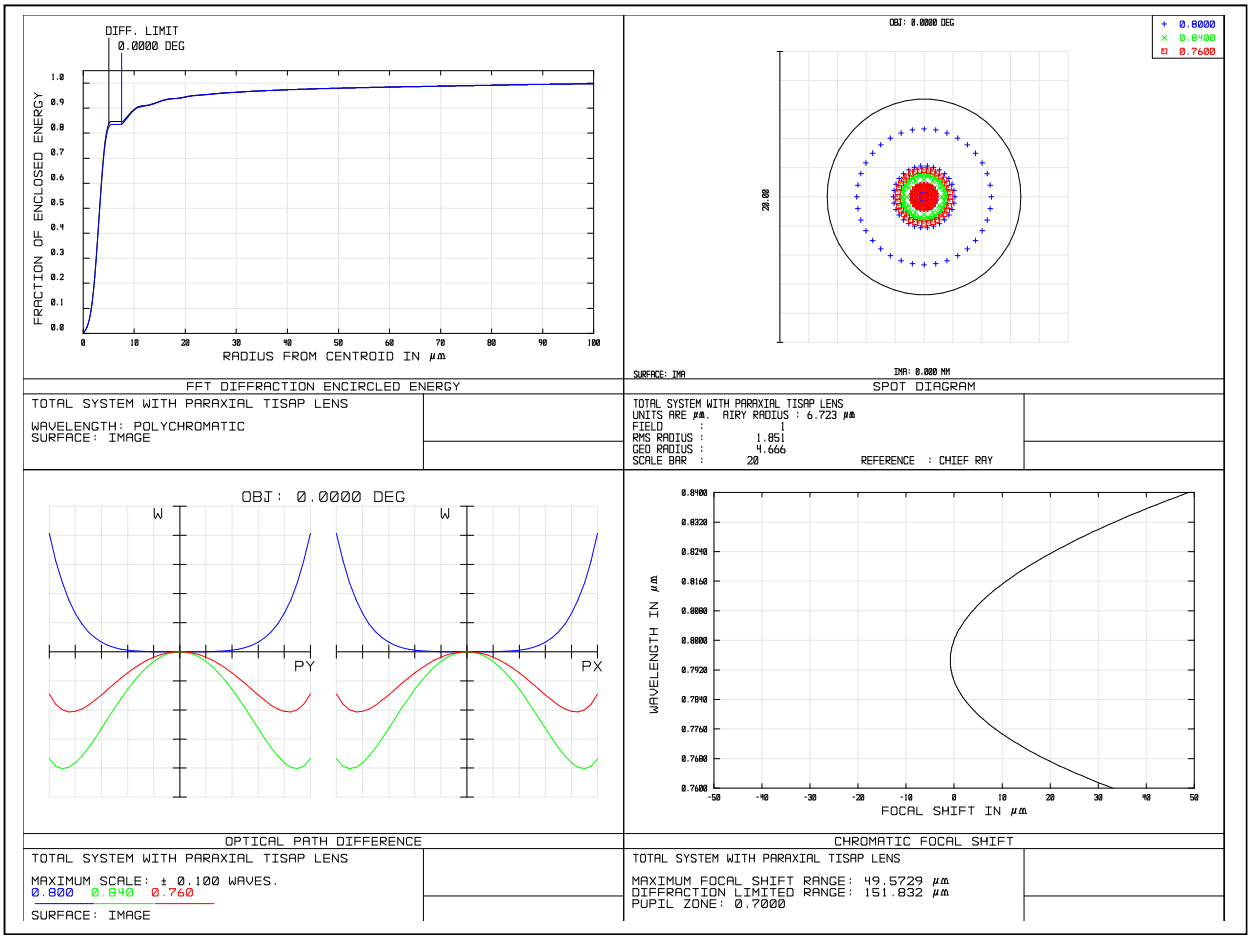

Figure 4. Zemax results report showing the encircled energy dependence (top left), multicolor spot size diagram (top right), OPD diagram (bottom left) and chromatic focal shift at the focus of a 1m lens for the case of the optimized lens separation with thermal lens in the Ti:Sapphire crystal.

compensation by a single AO mirror might be insufficient for our purposes because four passes through the Ti:Sapphire would produce a wave-front error of 100 waves. The error is predicted to have mainly parabolic radial dependence however (see figure 2) so could be easily compensated by re-collimating the beam using the lenses in the three image relay telescopes. The later scenario was further analyzed using Zemax optical design software.

Because the paraxial lens approximation correctly describes the thermal lens within a 50mm beam diameter (see figure 2), the thermal lens can be modelled by an additional paraxial lens in place of the Ti:Sapphire crystal. The results of the Zemax modelling are presented in figure 4. Compensation of the thermal lens effect has been achieved simply by reducing separations between the 2 m achromatic lenses currently used in the amplifier. It has been estimated that for a 36.7m focal length thermal lens, the image-relay achromatic lenses should have shorter separation by approximately 115mm. The actual optical design allows such changes to be made. The beam quality parameters after thermal lens compensation remain as good as before; the encircled energy diagram is close to ideal, and multicolor focal spots fall within an Airy ring of the ideal beam (see figure 4).

Conclusions

Results of computer simulation of thermal lensing in the Gemini Ti:Sapphire disc under a 10Hz repetition rate pumping and at room temperature cooling conditions are presented. Index matching liquid with light absorbing dye is essential for the suppression of parasitic lasing inside the Ti:Sapphire due to internal reflection at the crystal edges [3]. We therefore modelled the cooling of the crystal at room temperature so that this index matching liquid can continue to be used. It is confirmed that thermal lensing effect inside the laser crystal could be compensated by a simple beam re-collimation using existing optical elements. However, the compensating realignment of the optical system would require continuous pumping of the crystal to keep the system aligned. Therefore, a combination of AO and an adaptive beam re-collimation with lenses would be a good compromise for the room temperature case. In case when severe reduction of thermal lensing is required a low temperature cooling should be considered in the future designs.

References

1. K. Ertel, C. Hooker, J. Collier, CLF Annual report 2004-2005, p.217
2. O. Chekhlov, E.J. Divall, K. Ertel, S.J. Hawkes, C. Hooker, J. Collier, CLF Annual report 2005-2006, p.165
3. K. Ertel, C. Hooker, S.J. Hawkes, B.T. Parry, J. Collier, OPTICS EXPRESS 2008, Vol. 16, No. 11,8039

Development of dielectric-coated adaptive mirrors

Contact *chris.hooker@stfc.ac.uk*

Chris Hooker, Bryn T Parry and Luke Walker

Central Laser Facility
STFC Rutherford Appleton Laboratory

Introduction

Adaptive or deformable mirrors have been used in the high-power laser facilities at the CLF for many years. Previously, all such mirrors had metallic coatings, because coating the very thin substrates with a multilayer dielectric reflector leads to the substrate becoming severely curved by the internal stress in the coating. To overcome this, we have adopted the strategy of coating the substrate on *both* sides with the same coating, so that the stresses cancel out. The result has been a great success, in that a working deformable mirror with a dielectric coating, fabricated in-house, was demonstrated for the first time earlier this year.

Mirror fabrication

The same fabrication technique was used for these mirrors as described previously [1]. However, in order to ensure the technique would be successful, we had first to confirm that the piezo-ceramic material could be glued to the coated substrate, rather than to the fine-ground surface of the glass itself. We also had to check that the coating adhered sufficiently well to the substrate, and would not be pulled off the glass by the repeated flexing of the piezo during the operation of the mirror.

Both of these requirements were tested by gluing an old piezo-ceramic disc to a damaged 800 nm dielectric mirror with the same UV-curing adhesive that is normally used for assembling the mirrors. The discs were positioned with an offset, so each one overhung the other on one side, and then weights were placed on both so as to put the bond under tension. A load of 7 kg acting on one side did not separate the two materials during the course of a weekend, so we concluded that the adhesion between all the different materials was good enough for the purpose of fabricating a deformable mirror.

Six Pyrex substrates of 3 inches diameter and 2 mm thickness were available, so these were sent to an optical company for double-sided polishing and coating with a multilayer dielectric stack designed for 800 nm at 0 degrees. The intention was to make some test mirrors that, if successful, could be used on Astra in the expanded beam after Amplifier 3. At this position there is noticeable astigmatism on the beam that results from the four passes of a non-collimated beam through the Ti:sapphire crystal. Using an adaptive mirror to correct the aberrations before the beam is split to go to ATA2 would improve both the focusability of the beam in that area and the quality of the beam delivered to Gemini.

After coating, all six substrates were tested in reflection by using a shear plate in the Gemini CW diode beam. The fringes in the beam reflected from each face of the substrates gave a good indication that the double-sided coating technique had achieved the desired result, as the curvatures were relatively small (1 to 3 fringes) in five of the six parts. Previous tests of single-sided coatings had shown curvatures of 30 fringes or more. The sixth substrate was less successful, as its surfaces showed curvatures of 7 and 9 fringes. This substrate was selected as a test piece for the remainder of the fabrication processes, so that any problems that arose in processing could be identified without damaging one of the good substrates. A piezoceramic disc was glued to one side, and it was sent for grinding, with the front face coating being protected from abrasion by a layer of special lacquer. The grinding was successful, and the front face coating was not damaged during the process. On testing the curvature again, it was found to be seven fringes, exactly the same as in the first test, confirming that the fabrication process with double-sided coatings was a viable route to making dielectric deformable mirrors.

Two more piezo-substrate assemblies were made, and sent for grinding. Meanwhile, we tested a new method for applying the electrode pattern to the piezo after grinding.

Electrode fabrication

The previous method of forming the pattern of actuator electrodes on the back of the piezo slice required the ceramic to be spun with a layer of photoresist. This was exposed through a mask transparency having a pattern of lines corresponding to the desired gaps between actuator areas, and the lines were left on the piezo after the resist was developed. The masked plate was then sputtered with 1-2 microns of copper in the Target Fabrication laboratory. Washing off the photoresist left behind a pattern of islands of copper that were electrically isolated from each other.

To simplify the process we decided to avoid the photoresist step and evaporate the metal coating directly through a mask placed in contact with the piezo. Test coatings on blank substrates showed that the bars of the mask needed to be about 1 mm wide, in order to eliminate spreading of the deposited metal so that adjacent actuator areas remained electrically isolated. A mask pattern was fabricated in 0.3 mm thick stainless steel discs with the same diameter as the substrate. The bars in the masks were 1 mm wide, and the thickness ensured that the masks were sufficiently stiff to avoid them sagging away from the substrate and allowing the deposited metal to spread. A trial coating through the new masks on the test sample gave excellent results, with complete isolation between the deposited areas. The coated assembly is shown in Figure 1.

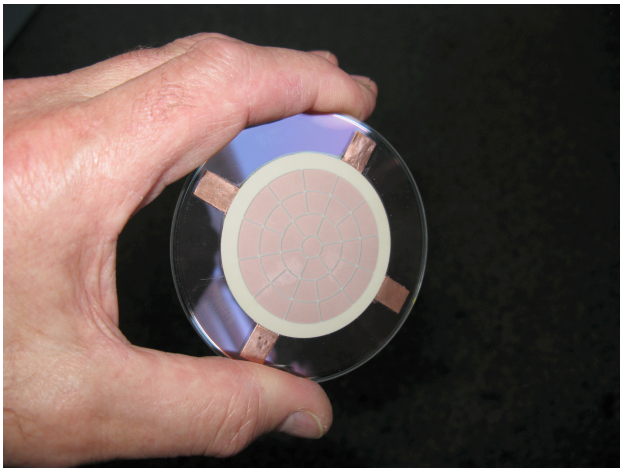

Figure 1. 3-inch adaptive optic assembly with coated pattern of copper electrodes on the piezoceramic disk.

Stress testing

One concern regarding dielectric coatings on deformable mirrors was that the repeated flexing could cause the coating to crack, and flake or peel off the substrate. To investigate this, all

the actuator areas on the test mirror were connected using silver paint, and a variable-frequency signal generator was connected between the linked electrodes and the ground plane. The signal generator produced a square-wave with a maximum peak-to-valley range of 10 volts. This is rather smaller than typical drive voltages; however, by adjusting the frequency to a mechanical resonance of the mirror and the mark-to-space ratio to 50%, the induced vibration had a maximum amplitude and was almost entirely due to the fundamental component at a frequency of around 500 Hz. If the frequency was tuned slightly away from the correct point, the third harmonic component also became audible, allowing a fairly accurate frequency setting to be made. A higher-frequency resonance was also found at around 3 kHz. The noise produced by the vibrating mirror was loud enough to be annoying, so the tests were mainly carried out over a weekend when no-one was in the laboratory. No effect on the coating was observed after several days of continuous operation at two different resonant frequencies. The coating was inspected under bright light to see whether there was any cracking or flaking, but no flaws were visible, so we concluded that the coating was sufficiently robust for use on a deformable mirror.

Mirror wiring

The connections to the electrodes of all the home-made AOs have been made using conducting (silver) paint to attach the bare ends of thin wires to the copper regions. The other end of the wire is soldered to a customized printed circuit board that accepts the drive cables from the driver box [Figure 2]. The wiring is a difficult and fiddly job, and an improved method of making the connections is under development. This is based on the use of spring contacts in an array that matches the actuator pattern, and will allow the easy replacement of the mirror plate if it becomes damaged. The current mirror, however, was wired as described and set up in the AO lab for testing.

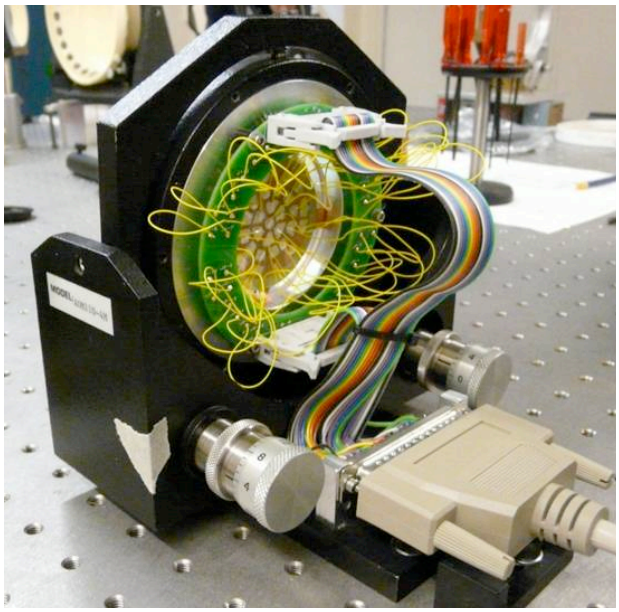

Figure 2. 3-inch adaptive mirror in mount, with custom-made annular circuit board and connectors, showing the wiring of the actuators.

Performance of the mirror

The assembled mirror was tested in the AO lab using the 800 nm CW diode beam, which was apertured to 32 mm to match the diameter of the beam in Astra that it will be required to correct. Once the response matrix had been determined, the dielectric mirror performed just as well as the previous mirrors with metallic coatings. It was easily able to correct its own residual errors, and could compensate for aberrations caused by poor-quality glass slabs inserted into the beam. Examples of uncorrected and corrected focal spots are presented in Figure 3.

Conclusions

A dielectric-coated deformable mirror has been constructed in-house, demonstrating the success of the double-sided coating technique in avoiding the severe curvature seen when the coating was applied to only one surface of the glass. The mirror performed just as well as metallic-coated mirrors made previously. One of the test mirrors made as part of this work will be installed in Astra during the next few months, in order to improve the optical quality of the beams sent to TA2 and Gemini.

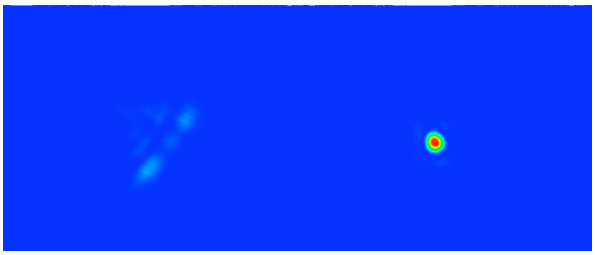

Figure 3. Initial and corrected far-field spots of an 800 nm CW diode laser beam, demonstrating the performance of the dielectric-coated adaptive mirror described in the text.

References

1. CLF Annual Report 2005-06, pp202-205

Monitoring Astra Gemini with penguin

Contact *victoria.marshall@stfc.ac.uk*

Dr. Victoria A Marshall

Central Laser Facility, STFC Rutherford Appleton Laboratory

Introduction

The Astra Gemini laser facility involves a large number of lasers and optical instruments, together with a team of Laser Operators to run it on behalf of visiting experimental scientists. There are upwards of 100 PCs to control the facility and create diagnostic data; these too need management. This article describes a web-based software suite named *penguin* which enables the various groups of scientists and experts to gain an overall view of the state of the facility, and details of its day-to-day running.

Data sources

The penguin suite incorporates data from a variety of sources (see figure 1):

i. Diagnostic data

Approximately 400 channels of diagnostic data are produced for each shot. The majority of these channels are singular values, but there are also 40 camera images and oscilloscope traces. Every few minutes, over 60 "daily" environmental data channels of readings are taken to monitor room temperatures, compression chamber vacuum levels, pump laser energies, control modes, gas system pressures and supplies. All data is produced by the various diagnostic PCs and fed into an ICAT 4.2 meta-database managed by STFC's Scientific Computing Department.

ii. Diagnostic data PCs

The shot-based diagnostic data is produced by 11 PCs, and the daily data by two additional PCs. All of these PCs are monitored using an on-board application which sends heartbeat information every three minutes to a central Oracle database. The heartbeat includes information about the applications running on that PC, last update times of various configuration files, disk space, and timeliness of that PC's data channels with respect to the last shot or the current time depending on whether that PC is producing shot or daily data.

iii. Network status

The Astra Gemini network is provided via a dozen network switches (hubs) and MOXA (networked device) controllers. Two Gateway servers enable access between the Astra Gemini network and the outside world. If any of these networked devices were to fail, control over the shutters and sliders along the beam line would fail, and/or shot data would be lost when control messages were not received. It is vital therefore to monitor these devices and check that they are responding to *ping* in a timely manner.

iv. Laser status data

The main laser control system orchestrates use of the laser in terms of who has control of the beam, and in which energy and pulse modes. It interfaces with the safety interlock system and provides definitive shot numbers and time-stamps, as well as controlling the positions of the various shutters and sliders along the beam line. A UDP feed to a separate application maintains a snapshot of these parameters every minute, and the results are fed into the Oracle database.

v. Experimental schedule, performance

Finally, a number of other data sources are used for miscellaneous purposes including an XML file containing the experiment schedule (which is also used by the ICAT system), and performance timings on the penguin applications themselves to monitor the health of the site network and the servers on which penguin depends.

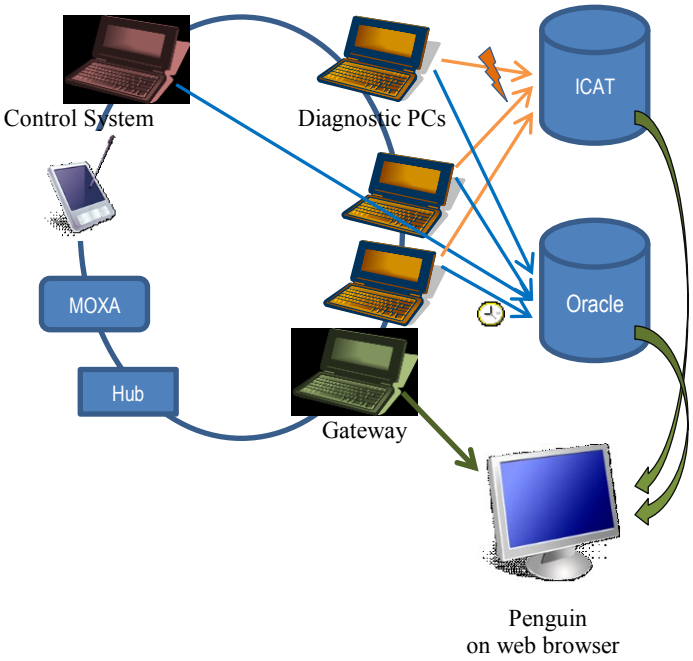

Figure 1: Schematic of the Astra Gemini network showing data sources.

Penguin applications

The penguin suite consists of a number of web-based Java applications which use JavaScript and SVG to present their data. These applications include:

a. Main operations

This is the main penguin application which provides an overview of the state of the beam line, laser parameters and diagnostic PCs. (Figure 2.)

b. Gas system

Astra Gemini recently commissioned a monitoring and supply system for gases used on the beam line as well as for experimental targets. A diagnostic application reads data directly from the Measurement Systems Ltd (MSL) DataWeb 4016 data acquisition systems and sends it to ICAT. Two penguin applications use this data to display the current state of the gas system (Figure 3) and plot that data over the course of the day (Figure 4).

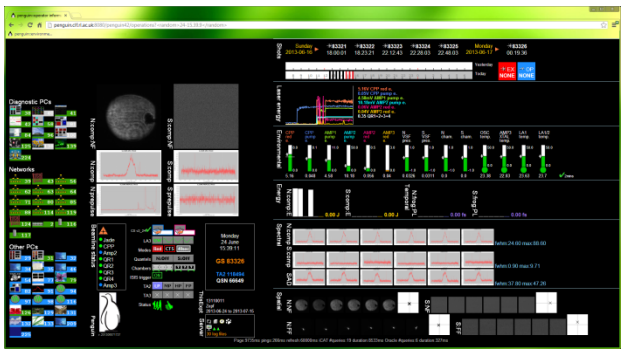

Figure 2: Penguin::Operations showing (on left) the status of diagnostic PCs, networked and other devices (all OK in this example); (centre) the latest compressed near-field image, spectral and pre-pulse traces, information about the energy modes in the different target areas (CW in LA3, LP in TA2), compression chamber vacuum status (North pumped down, South let-up), the current date, time and experiment; (on right) shots taken yesterday (none), today (several), a plot of pump energies over the course of today, gauges and thermometers for critical parameters (all within range), and the energy, pulse-length, traces, near- and far-field images for the last six shots.

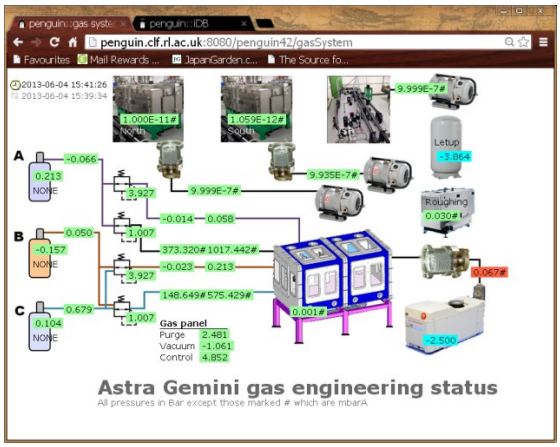

Figure 3: Penguin::GasSystem showing the current state of the gas system. All values are within range at the moment with the exception of the interaction chamber backing pressure. No experimental gases are currently in use.

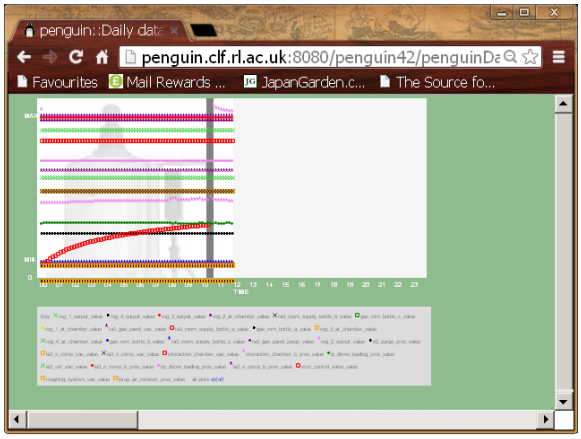

Figure 4: Penguin::DailyGas parameters so far today. Everything is holding steady while the interaction chamber is let-up. There were a few shots a couple of hours ago.

c. User logistics

As part of its operating remit, Astra Gemini is required to maintain records and provide statistics on the use of the facility. Another penguin application is available to users during the experiment which they can use to record the time they arrive, the time the leave, and any problems that occur. (Figure 5.)

Figure 5: Penguin::UserOperations showing that the beam is fully operational, that users have control, that the users have arrived and that there are no problems outstanding.

These events are logged in the Oracle database and can be analyzed at the end of the year to supply usage statistics. This includes laser availability throughout the experiment/year, time lost due to various problems on the beam line (and how quickly they were resolved!), and the length of time users were on site for Health and Safety reasons. The data are also available to the facility manager when compiling yearly statistics; problem/solution events and user comments can be combined with pump laser energies and control modes to calculate the percentage laser availability to the users. (Figure 6.)

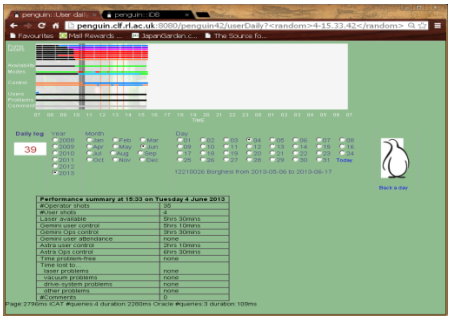

Figure 6: Penguin::DailyLog for today showing the pump lasers warming up, laser modes (mostly CW), and hand-over of control to the users. 39 shots were fired at about 10:30 this morning, and no problems have been reported.

Conclusions

Penguin is very much a work in progress. It has evolved considerably over the last few years as features are added or improved in response to requirements from the Operators "on the ground" and the IT manager, and in response to problems or near misses that could have been detected. The main Operations application is usually displayed on the 40" monitor in the Control Room, but because it is a web-based application there is scope for remote access to it via a browser (for anybody on-site) or mobile phone (for the IT manager). The combination of UserOperations and DailyLog has proved very invaluable to the Facility Operations Manager, and these were almost certainly used in the preparation of statistics in this annual report.

Acknowledgements

My thanks go to everyone in the Astra Gemini Operations team for all of their penguin suggestions.

Adaptive optic developments for the Astra Gemini target area

Contact *andrew.sellers@stfc.ac.uk*

A J Sellers, D R Symes, C J Hooker

Central Laser Facility, STFC Rutherford Appleton Laboratory, Harwell Campus, Oxfordshire, OX11 0QX

Introduction

The Astra Gemini facility allows for high intensity laser interactions through fast focusing optics and small focal spots. In order to achieve this desired outcome, the best possible quality of beam must be focused down. This means removing aberrations from the beam so that the wavefront is as flat as possible, before sending it to a parabolic mirror for focusing. Adaptive optic (AO) systems have been used to improve wavefront quality. Previously, a facility made deformable mirror (DM) was used in the target area to compensate for the deformities in the wavefront. In addition to this, a commercial option has been tested with Imagine Optic's Intense Laser Adaptive Optic (ILAO) mirror.

One of the main areas of interest was seeing how well the ILAO mirror coped with correcting for the presence of a thin mirror with a hole in it. The thin mirror is hoped to be used in an F/0.87 on-axis parabola setup which should achieve a smaller focal spot and higher intensities. By its very nature of being a thin mirror, it introduced a lot of aberration into the system so it was important to see if the ILAO could deal with this.

Equipment

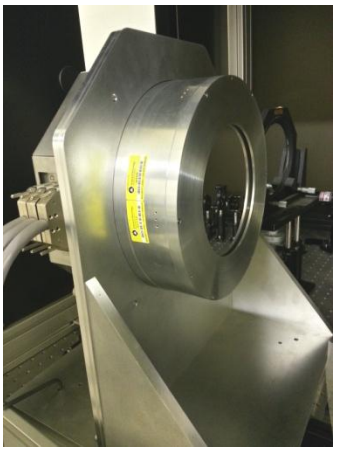

Fig. 1: The ILAO mirror

The mirror tested was an Imagine Optic ILAO 180 deformable mirror which can be seen in Fig. 1. It is comprised of 52 actuators in a circular pattern on the back of a thin metallic membrane. Whereas with previous DMs using piezoelectric actuators and needing a certain voltage to get to a certain position, the ILAO has mechanical actuators that move to apply a certain force on the mirror. With this method, once the actuators have been moved, they can remain at that position without requiring any more power.

Setup

Tests were made using a 150mm diameter, 632.8nm HeNe beam. This was reflected from the ILAO mirror to a thin mirror with an off-centred hole and then brought to focus with a 3.5m focal length lens. A 100mm lens was then used to make a telescope system so that a wavefront sensor could image the plane of the ILAO. Fig. 2 shows the basic arrangement of the setup used.

The wavefront sensor used to measure the shape of the beam was an Imagine Optic HASO3-32. It uses Shack-Hartmann technology with a 32x40 microlens array.

A mirror on a kinematic base was used to divert the beam towards a far-field CCD diagnostic so that the focus of the beam could be observed at different stages in the correction process.

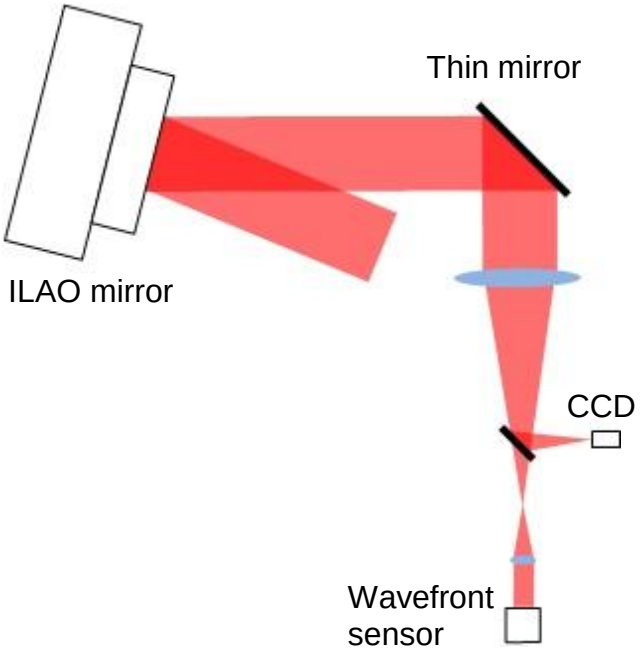

Fig. 2: Approximate setup of optics used for testing

As the ILAO mirror may have not been in an exactly flat position from the factory and the thin mirror is not flat, the presence of these optics in the setup introduced deformities into the beam. Therefore the beamline was firstly set up without these and had regular 235mm sliver mirrors instead. Fig. 3 shows their effects on the beam can be seen by looking at the far-field before and after the mirrors have been put in the system. We can see from this the work that needs to be done by the ILAO to correct the beam.

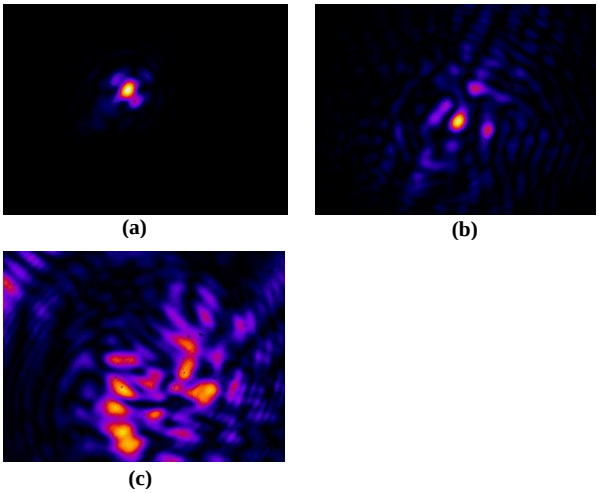

(a) **(b)** **(c)**

Fig. 3: Focal spot with (a): All regular mirrors, (b): Just ILAO mirror added, (c): ILAO and thin mirror

Method

Imagine Optic's CASAO software was used to control the ILAO and communicate with the HASO sensor to see the state of the wavefront. Once the beam was aligned onto the wavefront sensor, a standard AO correction procedure was performed. Firstly, influence functions are gathered from the mirror. Each actuator is pushed and pulled by a certain amount and its influence on the shape of the rest of the mirror is observed. Depending on the configuration, this process can take between 10 and 20 minutes to complete. When the mirror has finished, there is now an interaction matrix of what the actuators can achieve to change the wavefront. This is then converted into a command matrix so that the mirror can move into the best possible position to give a flat wavefront. It takes a few iterations of moving the mirror and looking at the resulting wavefront to get to the desired outcome.

Correcting Full Beam

Before using the thin mirror in the beam, a regular silver mirror was put in its place so the ILAO mirror could be tested with a complete circular beam and no hole in it. After putting just the ILAO in the beam, the wavefront was measured and is shown in Fig. 4. The HASO also shows aberration values for corresponding Zernike polynomials which can be seen in Fig. 5. We can see that there are high levels of aberrations and the focus of the beam, Fig. 6, is not of good quality with lots of light being lost outside the central point.

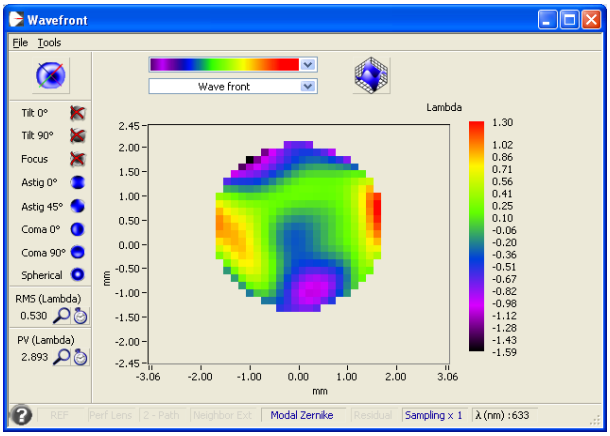

Fig. 4: The wavefront of the beam after the ILAO mirror was added to the setup.

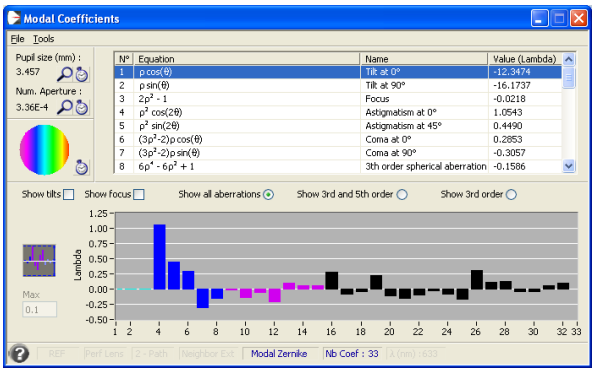

Fig. 5: Values for Zernike terms of the wavefront after adding the ILAO mirror.

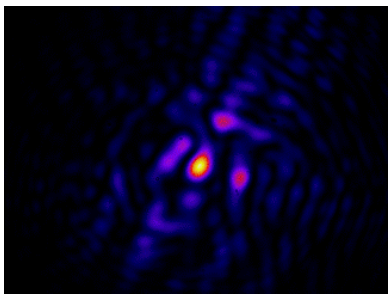

Fig. 6: Focal plane after adding the ILAO mirror

Fig. 7 shows the best correction seen so far from the ILAO mirror. It can be seen that the mirror has very good correction capabilities, correcting for its own original state and improving the original beam further. Note the difference in scale for the Zernike polynomial values in Fig. 8.

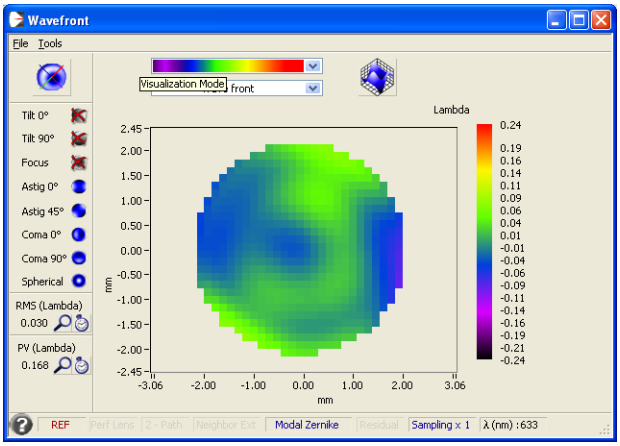

Fig. 7: Wavefront after full beam correction

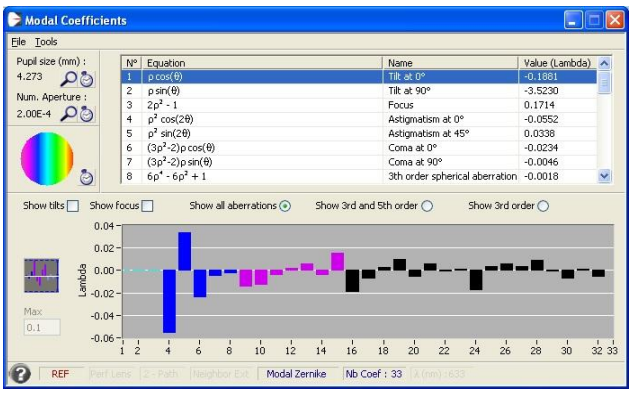

Fig. 8: Zernike values after full beam correction

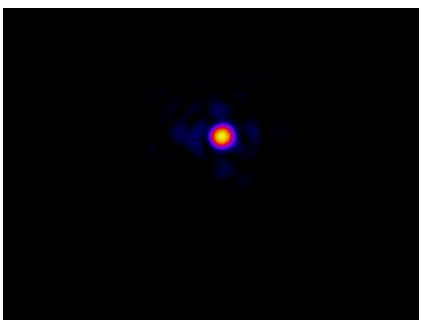

Fig. 9: Focus after full beam correction

Fig. 9 shows how the ILAO has greatly improved the focal spot, containing the light within a uniform central spot.

Correcting Thin Mirror

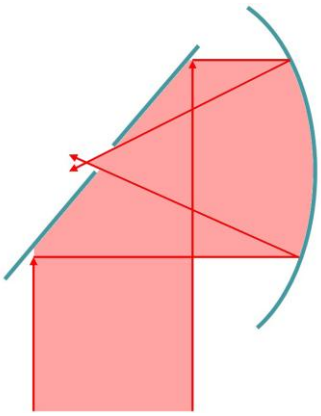

Fig. 10: Planned arrangement of thin mirror and on-axis F/0.87 parabola

The planned arrangement for the thin mirror with the on-axis F/0.87 parabola can be seen in Fig. 10[1]. However, for the purposes of testing, the thin mirror was still used with the 3.5m focal length lens. Fig. 11 shows what the wavefront looked like on the HASO wavefront sensor. It can be seen that some of the information about the shape of the wavefront was lost due to the hole in the thin mirror. This means there couldn't be any measurements made for Zernike values as this requires a full circular area to be measured with no missing information. However, the HASO still gives a measure of the peak-to-valley (PV) of the wavefront and the root mean squared (RMS) of the height differences in the beam.

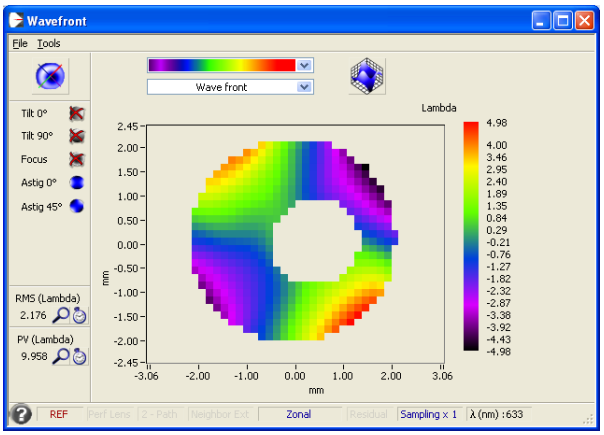

Fig. 11: Wavefront of the beam after the thin mirror was added.

The camera signal can be seen in Fig. 12. Each bright point is a focused sub-pupil for the microlens array and it's the subtle change of the positions of these sub-pupils that help the HASO make its measurements. As the hole in the mirror is off centred, this means there are less sub-pupils between the edge of the hole and the edge of the mirror, which means there is less information being provided for this section of the beam.

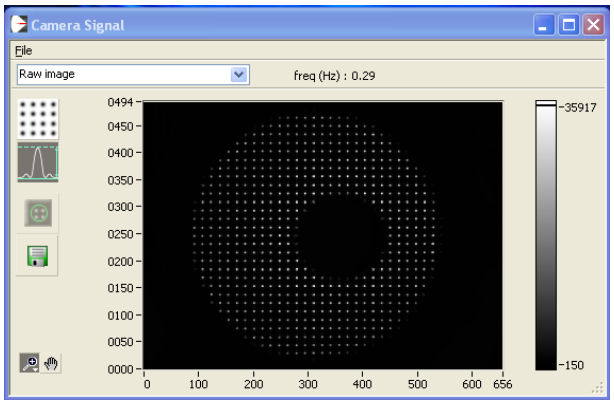

Fig. 12: Camera signal on wavefront sensor, showing sub-pupil array.

A correction of the beam was then performed. Below, Fig. 13 shows the resulting wavefront. It can be seen that the mirror has improved the wavefront greatly as it started with a difference of over 2 waves RMS and has ended up at about a tenth of a wave RMS. The ILAO mirror has corrected well for the large amount of deformities produced by the thin mirror and has achieved this despite the loss of information due to the hole in it.

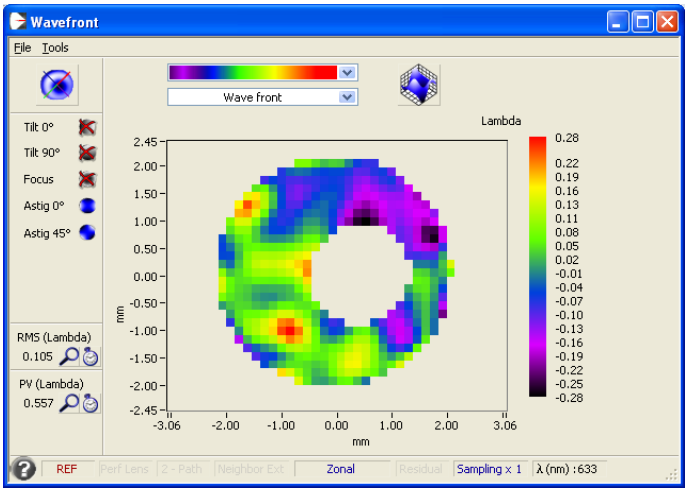

Fig. 13: Wavefront after thin mirror correction.

Fig. 14 (a) shows how bad the far-field looked like before correction. This has changed from Fig. 3 (c) as the mirror's starting position was the final position from the full beam correction. The light didn't converge to a central point at all so the picture shows the location of least confusion. The corrected focal spot can be seen in Fig. 14 (b). The light has now converged to a focal spot with an airy ring around it.

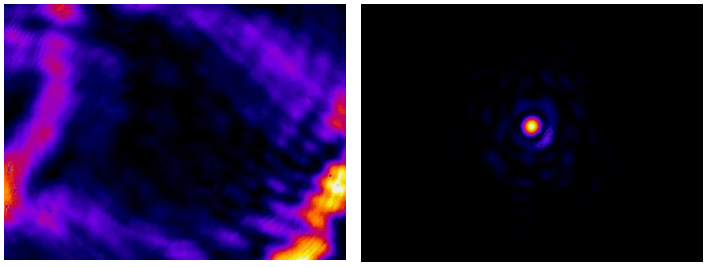

(a) **(b)**

Fig. 14: (a) Focal plane before correction, (b) Focal plane after correction.

Results

	Encircled Energy / %	
	FWHM	$1/e^2$
Off regular mirrors	29	53
After full beam correction	38	65
After thin mirror correction	33	52

Table. 1: Different encircled energy results before and after corrections

Table 1. shows the values for the encircled energies, in the full width half max and $1/e^2$ limits, for the different focal spots throughout the testing. A good correction can be seen for the full beam, showing that the ILAO mirror can compensate for its own presence and improve the beam further. Considering that there wasn't a focal spot at all when the thin mirror was introduced, the ILAO mirror has done very well to improve the encircled energy in the FWHM from regular mirrors and to keep the $1/e^2$ value similar.

Conclusions

The new ILAO mirror has been tested for correcting capabilities of a full aperture beam and also for the presence of a thin mirror with an off centred hole. For a full beam setup, it has performed well in flattening the beam and reducing the values for the Zernike terms associated with circular beams. It has also managed to increase the encircled energy within the focal spot which was a desired outcome.

Great improvements have been seen in compensating for the highly aberrating thin mirror. The light started out totally dispersed at the focal plane but the ILAO managed to converge the light to a central spot. This is a good development as the previous AO setup found it difficult to cope with deformities of the thin mirror and the annular correction due to the hole in the thin mirror.

One improvement to corrections that could be made would be to use a higher resolution wavefront sensor. As mentioned earlier with the help of Fig. 12, there are less sub-pupils between the hole and one side of the mirror as the hole is off-centred. Therefore there is less information there about the wavefront. A higher resolution wavefront sensor would have a bigger chip and more sub-pupils to give information about what the beam looks like between the hole and the edge of the mirror. This will be the next test for the thin mirror setup.

The ILAO mirror is quite large in size so would take up more space in the target chamber. Facility users who would like this in their setups would have to factor in its large size as it would leave less space for other potential beam paths.

References

1. J D Alston, P S Foster, M Galimberti, C J Hooker, R P Pattathil, K Poder, D R Symes, CLF Annual Report 2013, pp 49

Implementation of adaptive optics on the Astra-Gemini beamlines

Contact *dan.symes@stfc.ac.uk*

D. R. Symes, A. J. Sellers, S. J. Hawkes, J. D. Alston, C. J. Hooker, O. Chekhlov, B. Parry, Y. Tang, M. Galimberti, N. Booth, P. S. Foster, P. P. Rajeev

Central Laser Facility, STFC Rutherford Appleton Laboratory, Chilton, Didcot, OX11 0QX, UK

K. Poder, J. M. Cole, N. C. Lopes

The John Adams Institute for Accelerator Science, Blackett Laboratory, Imperial College London, SW7 2AZ, UK

Introduction

To achieve high powers, lasers are required to have large beam areas and so it is a challenge to maintain a high quality wavefront. Since it is also essential to achieve the best possible focal spot, adaptive optics are required to compensate for aberrations inherent to the laser system. The rapid development of both laser and adaptive optic technology has led to modern commercial systems incorporating these devices as a default. This year we have installed full size adaptive optics in both beamlines of Astra-Gemini in Target Area 3 in order to improve operational delivery.

Arrangement for *f*/20 beamline

For the *f*/20 beamline we used a gold mirror produced in-house which uses piezoelectric actuators to deform the surface [1]. It is placed into the beamline before the final turning mirror onto the parabola. As part of the daily alignment procedure an uncoated wedge is driven into the beam directing it out of the chamber through a 1mm thick window. A lens is used to collimate the beam and image the plane of the adaptive optic onto a HASO wavefront sensor. The wavefront is optimized using the CASAO software package from Imagine Optic [2]. The wedge is then removed and the focal spot observed using a 10x magnification objective lens. Because of aberrations in the reference line, the focal spot may need slight adjustments which can be applied while directly looking at the focus, which is possible because of the rapid response of the piezoelectric actuators. This also means that aberrations can deliberately be added to the focus using the software. This method has been used on two experiments and will become our standard routine for *f*/20 campaigns.

Arrangement for *f*/2 beamline

For the *f*/2 beamline we have installed the Intense Laser Adaptive Optics (ILAO) deformable mirror from Imagine Optic [2] for the experiment being conducted at the time of writing. This has been developed specifically for intense lasers and uses mechanical rather than piezoelectric actuators and so can be unpowered once the desired mirror shape has been set. It is more difficult with the fast focusing parabola to collect the beam for a reference arm for wavefront optimization so instead we diverted the beam outside the chamber at the last convenient location in the beamline. This means that there may be slight aberrations from the final steering optics and in future we may review this method. The CASAO software is again used to optimize the wavefront based on a measurement with the HASO sensor. Following this, the *f*/2 parabola is adjusted to minimize astigmatism in the focus visualized with a 50x magnification objective lens. Because the incoming wavefront is flat, this procedure corrects for misalignment of the parabola rather than compensating for aberrations in the beam (apart from the final steering optics).

Optimization results

(a)

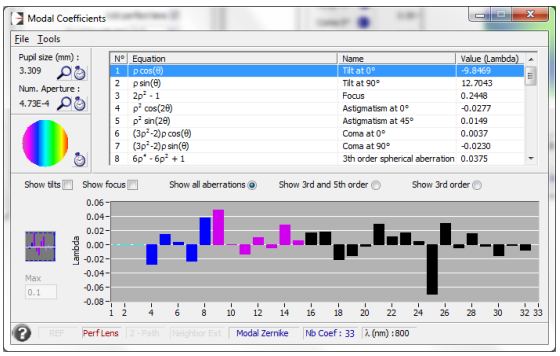

(b)

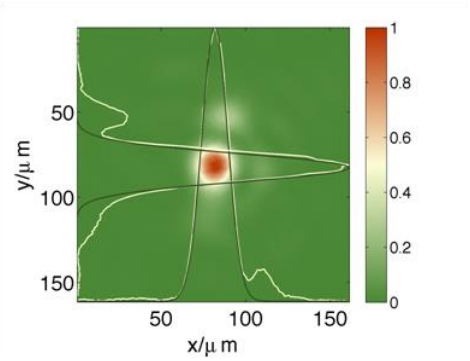

Figure 1. Wavefront and focal spot achieved using the CLF adaptive optic and *f*/20 parabola.

Figure 1(a) shows Zernike coefficients for the optimized wavefront achieved with the South beam after the *f*/20 parabola using the CLF adaptive optic. This has 0.038λ RMS variation across the beam and produces the focus in Fig. 1(b) with a spot radius ($1/e^2$) of w_0=16.7μm [3]. The energy contained under the correspondent gaussian fit is 56.9% compared to a theoretical maximum (for a top hat beam profile) of 76.6%. In Fig. 2 we display focal spots obtained when we add varying degrees of coma and spherical aberration.

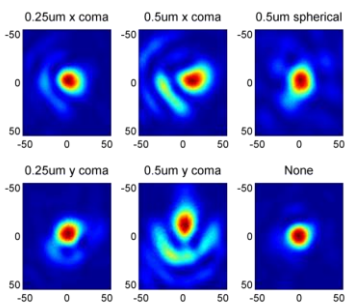

Figure 2. Focal spots obtained with the *f*/20 parabola with varying degrees of coma and spherical aberration. The optimized focus is shown in the bottom right panel.

The Zernike coefficients of the North beam corrected with the ILAO are shown in Fig. 3(a). In this case the RMS variation is 0.068λ, with λ/10 astigmatism remaining. It is possible that with further optimization we will be able to improve this. The corresponding focal spot using the *f*/2 parabola is shown in Fig 3(b) which has a spot radius ($1/e^2$) of w_0=1.6μm and contains 47% of the energy. The increase in energy outside the central spot compared to the *f*/20 might have been caused by the method used to attenuate the beam in this measurement. This will be investigated further at a later date.

(a)

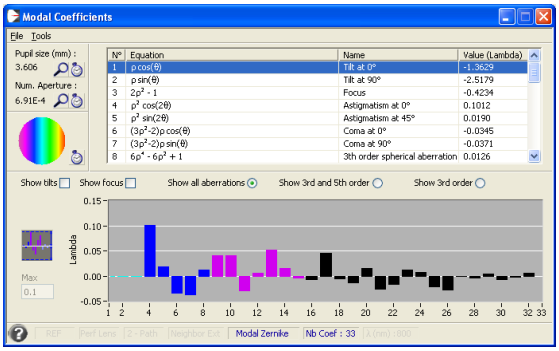

(b)

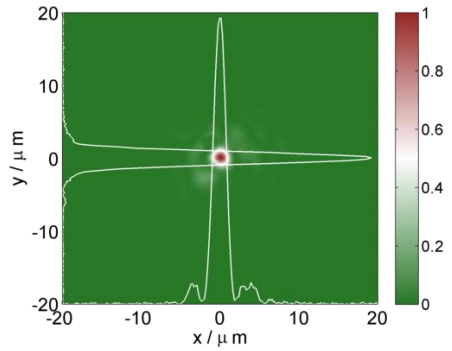

Figure 3. Wavefront and focal spot achieved using the ILAO and *f*/2 parabola.

The latest version of the HASO software which we used for the ILAO installation is able to generate a point spread function from the measurement and this is plotted in Fig. 4. As can be seen the focal spot quality is good with a Strehl ratio of 0.843. This reconstructed focal spot closely resembles the *f*/20 measurement with a partial Airy ring visible around the central spot.

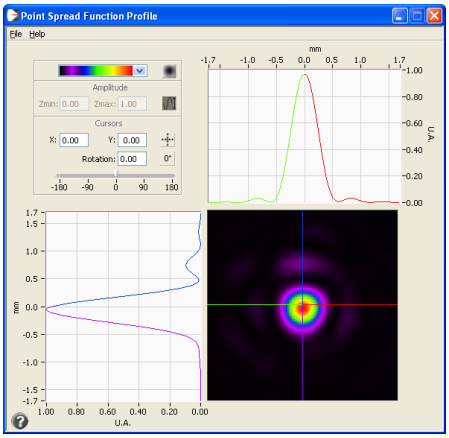

Figure 4. Predicted focal quality from HASO software (the units on this plot are not relevant).

Conclusions

We have implemented adaptive optics on the Astra-Gemini beamlines to improve the quality of the focal spot in both our standard focusing geometries. These optics have been successfully fielded on several experiments using the *f*/20 parabola and we aim in the next year to introduce the ILAO in routine operations with the *f*/2 parabola.

Acknowledgements

We thank the staff of Imagine Optic and Acal BFi for very helpful discussions and training in the use of the ILAO.

References

1. J. D. Alston, P. S. Foster, M. Galimberti, C. J. Hooker, R. P. Pattathil, K. Poder, D. R. Symes, *CLF Annual Report 2012*, pp 49
2. www.imagine-optic.com
3. N. C. Lopes *et al*. in this CLF Annual Report

Modified Cross-correlator for use on Beam Combination Experiment

Contact *alexis.boyle@stfc.ac.uk*

Alexis Boyle, Marco Galimberti, Jonathan Phillips

Central Laser Facility, STFC Rutherford Appleton Laboratory
Chilton, Didcot, Oxon. OX11 0QX

Introduction

Here we report a modified near field (NF) autocorrelator (AC) for measuring the cross correlation of two recombined beams. The Astra-Gemini laser has two half petawatt beams that are seeded from the same pulse. The cross correlator was built to measure AC of both beams and a cross correlation of the combined beam to prove the recombination.

Design

The cross correlator was built from a modified NF AC design currently on use in the Vulcan laser system. The beam splitter was changed for a D shaped mirror.

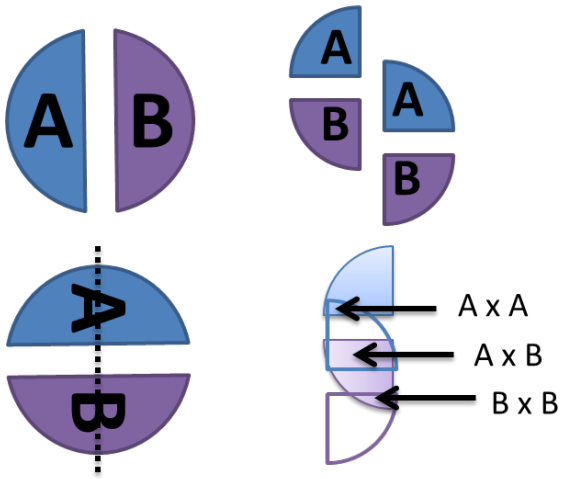

Figure 1: NF of the two beams to be combined (top left). Sampling the beams using the D shaped mirror, denoted by the dotted line (bottom left). Spatially offsetting the two NF in each arm of the cross correlator (top right). AC of beam A and B and cross correlation of A and B (bottom right).

Figure 1 shows the way that all three traces can be captured on the single shot NF AC. A sample is taken from the combined NF of beam A and B. This was done using a pick off mirror and relayed outside the target chamber. The orientation of the NF was then rotated by 90 degrees using a periscope setup. The D shaped mirror creates two NF samples to be cross correlated. The NF in each arm were vertically offset on the AC crystal resulting in three traces: an AC of A, an AC of B and a cross correlation of A and B in the center. Both AC act as fiduciary markers and the cross correlation should appear in line with these when the timing of the combined pulses matches.

Results

Figure 2 shows three separate measurements. The first two images prove that the ACs of A and B exist independently of one another. The bottom image shows all three single shot traces, when the timing of A and B overlap. This single shot image proves that for this shot both beam A and B where combined spatially and arrived on the device at the same time.

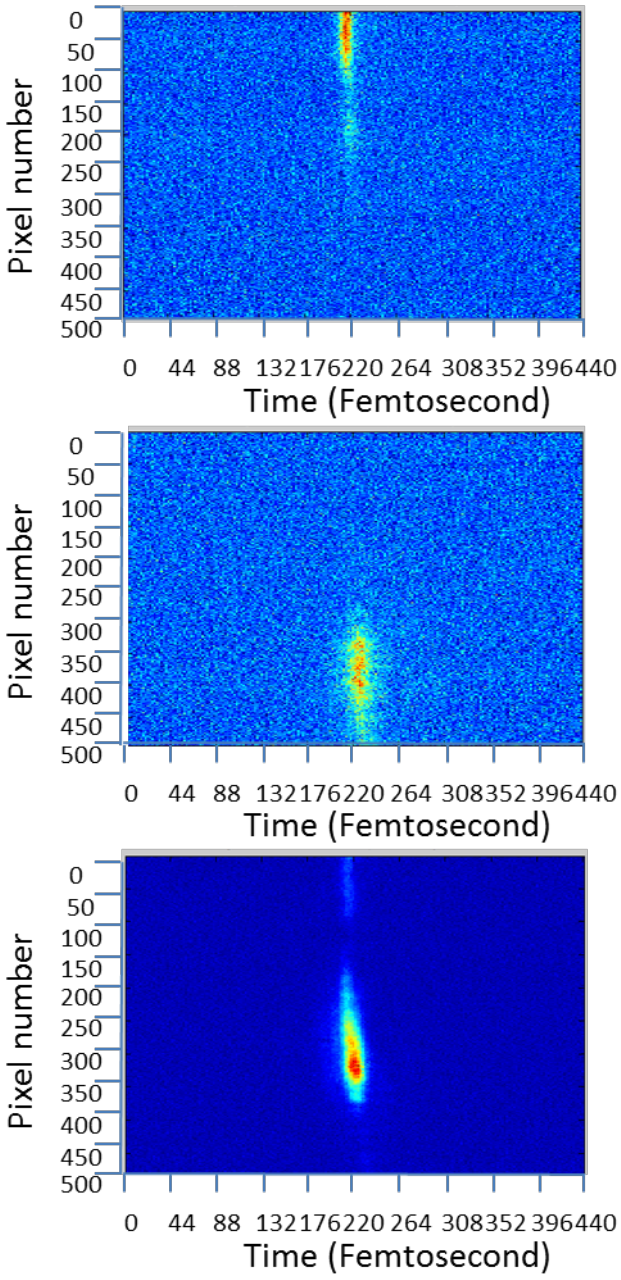

Figure 2: AC of A (top), AC of B (middle) and both AC and a cross correlation of A and B (bottom).

Conclusions

Here we present a modified NF AC device that is capable of providing three separate AC and cross correlation on the same single shot measurement. The single shot captured in figure two is shown to be temporally and spatially combined.